JOURNAL OF AIRCRAFT
Vol. 43, No. 6, November–December 2006

# Analysis and Wind Tunnel Testing of a Piezoelectric Tab for Aeroelastic Control Applications

Sebastian Heinze*
*Royal Institute of Technology, 100 44 Stockholm, Sweden*
and
Moti Karpel†
*Technion—Israel Institute of Technology, 32000 Haifa, Israel*

DOI: 10.2514/1.20060

**A concept for exploitation of a piezoelectric actuator by using aeroelastic amplification is presented. The approach is to use the actuator for excitation of a tab that occupies the rear 25% of a free-floating trailing edge flap. A flexible high aspect ratio wing wind tunnel model is used as a test case. Wind tunnel experiments were performed to determine frequency response functions for validation of the numerical model used for the control law design. The aeroservoelastic model is based on state-space equations of motion that accept piezoelectric voltage commands. Control laws are derived for gust alleviation with flutter and control authority constraints, and numerical results that demonstrate a significant reduction in the structural response are presented. Possible applications and feasibility of the concept are discussed.**

## Introduction

PIEZOELECTRIC materials have been in the focus of aeronautical research for many years [1–3]. Especially high bandwidth and small size are beneficial properties that allow for excitation that is not possible with conventional electric or hydraulic actuators. Recent applications of piezoelectric materials are found in aeroelastic and vibration control [4–7] as well as in the excitation of structures for the purpose of, for example, parameter identification [8]. Despite a wide range of applications, however, these materials are mostly used in research, rather than in real aircraft structures. Two of the main reasons for this are the relatively low actuator stroke and allowable strains.

The focus of this study is on the efficient exploitation of the advantages of piezoelectric materials, that is, small size and high bandwidth, while placing the actuator in a low-strain area and trying to compensate for the low stroke by aeroelastic amplification. This is done by using the piezoelectric material for excitation of a tab connected to a floating control surface, rather than controlling the surface itself. Aerodynamic amplification using trailing edge tabs is widely used in static applications, such as elevator trim tabs, and has been proven very efficient. In this study, the dynamic aeroelastic response of such a tab under piezoelectric actuation, when the flap is floating and does not have other actuators, is investigated.

The study is performed within the project Active Aeroelastic Aircraft Structures (3AS) [9], which is funded by the European Union under the Fifth Framework Programme.‡ As a test case, a high aspect ratio wing (HARW) wind tunnel model built within the project is considered. The wind tunnel model is a generic model of a high-altitude long-endurance surveillance aircraft wing that has been developed for a drag minimization study [10] and was modified for integration of the piezoelectric actuator.

## Experimental Setup

Experiments were performed in the low-speed wind tunnel L2000 at the Royal Institute of Technology (KTH) at airspeeds of 25 m/s at atmospheric pressure and room temperature. The 1.6 m semispan model is mounted vertically in the wind tunnel floor. In the current configuration, the wing consists of ten aerodynamic sections, one of which is equipped with the piezoelectric tab, as shown in Fig. 1. The stiff sections are clamped to a slender load-carrying flexible beam in a way that minimizes their contribution of stiffness to the structure.

A cross-sectional view of the section containing the piezoelectric actuator is shown in Fig. 2. The actuator mechanism is mounted to a frame within the floating trailing edge flap. Voltage excitation of the bimorph lead zirconate titanate (PZT) actuator results in vertical deflection at the actuator tip, located halfway between the flap hinge and the tab axis, leading to angular deflection of the tab, as shown in the sketch. The QP25N PZT actuator [11] was used in this study. The device is restricted to the maximal input of 100 V which yields, according to the manufacturer, a maximal peak-to-peak free displacement of 1.42 mm or the maximal zero-to-peak blocked force of 0.32 N, from which the piezoelectric and stiffness properties are extracted below. Because of mechanical restrictions, the maximum deflection of the control surface is less than 3 deg. It should, however, be noted that the focus is on amplification of this deflection by the floating flap, rather than on implementing an actuator mechanism featuring large deflections.

The objective of the experimental investigations was to derive frequency response functions (FRFs) relating dynamic tab deflections to structural response. The piezoactuator was therefore excited with a sine wave generator at several frequencies, and the structural response was measured using accelerometers located inside the wing as shown in Figs. 1 and 2. The main purpose of having accelerometer no. 4 is to extract the flap motion from accelerometer no. 3.

The tab deflection could not be measured directly during the experiments. Therefore, strain gauges were attached to the piezoactuator, and the strain in the actuator skin was considered to be a measure for the actuator tip displacement, which could be related to the tab deflection. The entire setup was calibrated statically, and it was found that due to fairly low inertial and aerodynamic loads on the tab, this calibration was sufficient for the frequency range considered here (up to 20 Hz). Accelerations and piezoelement strain were measured simultaneously to guarantee that there was no time delay between the signals. Experiments were performed with both the

Presented as Paper 150 at the CEAS/AIAA/DGLR International Forum on Aeroelasticity and Structural Dynamics 2005, Munich, Arabella Sheraton Grand Hotel, Germany, 28 June–1 July 2005; received 3 October 2005; revision received 26 April 2006; accepted for publication 2 May 2006. 

*Ph.D. Student, Department of Aeronautical and Vehicle Engineering, Division of Flight Dynamics, Teknikringen 8.

†Professor, Sanford Kaplan Chair in Aerospace Engineering, Faculty of Aerospace Engineering. Associate Fellow AIAA.

‡Homepage: www.3as.org.

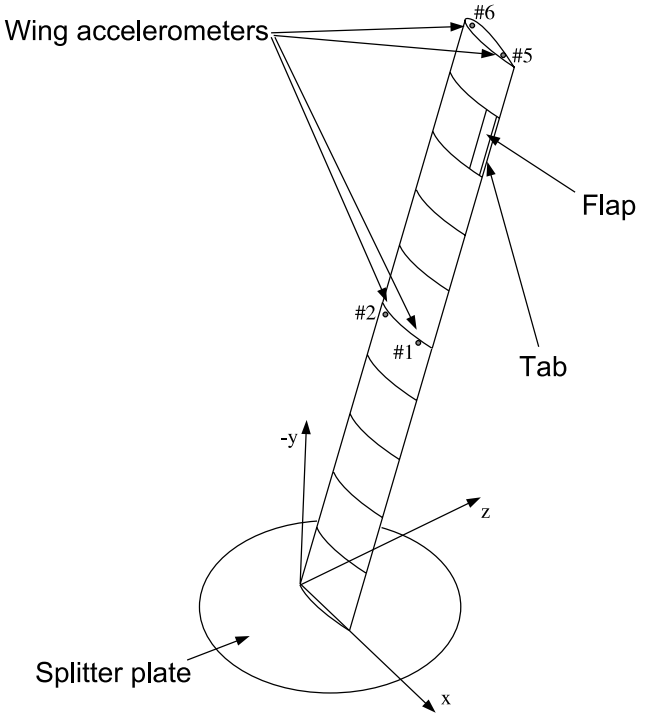


**Fig. 1 Experimental setup. The accelerometers are located inside the model.**

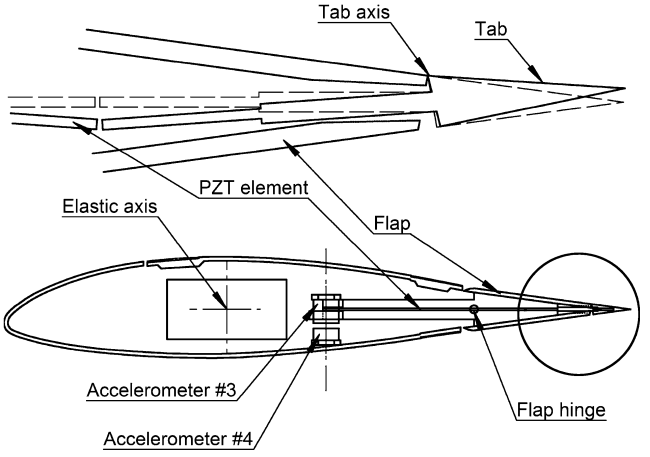


**Fig. 2 Cross-sectional view of the section with a piezoactuated tab.**

floating flap and with a locked flap to investigate the amplifying effect of the floating configuration. Note that the floating flap is not perfectly free due to cables connecting the PZT element to the rigid aerodynamic section.

## Numerical Modeling

*Nastran:* A numerical model of the wind tunnel wing was developed in MSC/Nastran [12]. Beam elements were used for modeling of the load-carrying spar. Structural properties were derived from material data and adjusted to both static experiments and vibration tests of the beam without the sections applied. Mass properties of the sections were derived from measurements and known material properties. Since each of the sections is attached to the beam in one point only without stiffness contribution to the beam, the sections were simply modeled as concentrated mass elements. The structural properties were finally validated by vibration tests with all sections applied to the clamped wing.

The flap was given some stiffness and damping in the rotational degree of freedom to account for cables connected to the piezoactuator. Even though the rotational stiffness is fairly low, it was found necessary for correct modeling of the flap dynamics. Throughout this paper, this configuration will be referred to as the stiffened configuration, as opposed to the free-floating case referring to the perfectly free flap. The flap and tab kinematics were described as multipoint constraints such that the flap deflection relative to the wing and the tab deflection relative to the flap appear as independent structural degrees of freedom.

Since MSC/Nastran does not facilitate for piezoelectric elements, the numerical model validation by comparisons with measured FRFs was performed with the tab deflection degree of freedom loaded with a large inertia of $10^4$ kg $\cdot$ m$^2$. In this way, the acceleration response to a sinusoidal moment excitation at this point with the amplitude of $10^4$ N $\cdot$ m is equal to the displacement FRF to tab deflection excitation. The disadvantage of this modeling is that tab dynamics are ignored, which did not cause a significant error in the frequency range of interest of our case. Flutter analyses were performed in the validation process with a locked tab.

A different approach to the tab modeling was taken in the generation of the Nastran structural model for the subsequent construction of an aeroservoelastic (ASE) numerical model for the design of a gust-alleviation control system, following the modeling approach of Karpel and Moulin [5]. Three collocated grid points, rigidly interconnected in all directions except $z$, were placed at a location that represents the tip of the PZT actuator. The $z$ displacement of the first point ($z_1$) was constrained to be the average of those on the hinges of the flap and the tab. The $z$ displacement of the second point ($z_2$) was connected to $z_1$ through a linear spring with the stiffness coefficient $k_v = 450.7$ N/m that reflects the actuator properties given above. $z_2$ was also constrained to $z_3$ and the electric input by the multipoint constraint (MPC) equation

$$z_2 = z_3 - x_v v$$

where $v$ is the translation of a scalar point that was added to the model to represent the voltage input. With $x_v = 7.1$ $\mu$m/V, a unit translation of the scalar point (representing $v = 1$ V) causes actuator displacements and forces that are consistent with the given piezoelectric characteristics and the dynamics of the surrounding structure [5]. Finally, $z_3$ was connected to the tab rotation degree of freedom using a rigid element.

The PZT actuator modeling is completed by loading the scalar displacement $v$ with a large fictitious mass of $M_H = 10^6$ kg. Normal modes analysis with the resulting model yields a rigid body mode of tab deflection only. This mode is to be used as the control mode in the subsequent aeroservoelastic analyses described below. The remaining frequencies and mode shapes are practically identical to those that would be obtained by adding the constraint $v = 0$, which represents the actual structure. These modes are slightly different than those obtained for the Nastran FRF analysis described earlier because the model now contains the tab mass and stiffness properties. The resulting tab natural frequency is 29 Hz, significantly above the frequency range of the important aeroelastic activity shown below.

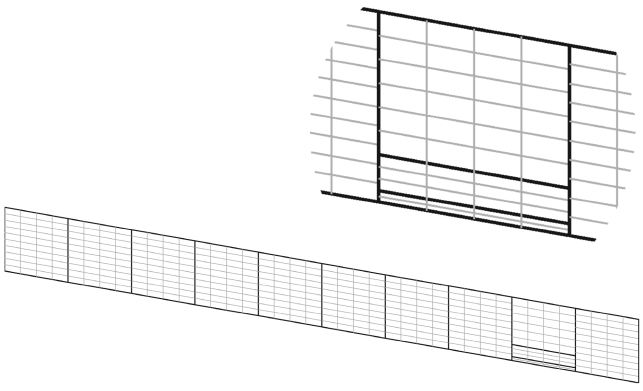

**Fig. 3 Aerodynamic mesh.**

The new Nastran modes were exported for subsequent stability and response analyses using ZAERO (see below).

Doublet-lattice aerodynamics [13] were used for computing the aerodynamic influence coefficient matrices for the Nastran FRF analyses. Aerodynamic panels were defined on each of the sections as shown in Fig. 3 and splined to rigid body elements transferring the aerodynamic loads to the structure in the attachment points. On each of the sections, four spanwise and 10 chordwise aerodynamic panels were used. On the second outermost section, 11 chordwise panels were defined, where six were placed on the section, three on the flap, and two on the tab.

The total number of panels used for the half-span wing became thus 404. The number of panels in the chordwise direction was doubled, and it was found that the results changed only marginally. Therefore, the number of panels was considered sufficient.

*ZAERO:* The Nastran normal modes with the detailed PZT actuator were used for generating the numerical model for ASE analysis and design using the ZAERO software package [14]. As discussed previously, the first normal mode was used as a control mode that generates the aerodynamic and inertial forces due to the activation of the PZT device. Nine elastic modes, up to 37 Hz, were taken into account, which resulted in 18 structural states. The frequency-domain aerodynamic coefficient matrices were generated by the ZONA6 option of ZAERO based on the same paneling as used for the FRF analysis in Nastran. A column of gust loads was added to the aerodynamic matrices to represent the load distribution due to sinusoidal gusts normal to the wing. The minimum-state aerodynamic approximation technique [15] was used to approximate the resulting generalized aerodynamic matrices as rational functions of the Laplace variable $s$, such that a state-space time-domain ASE model could be generated with four aerodynamic lag states.

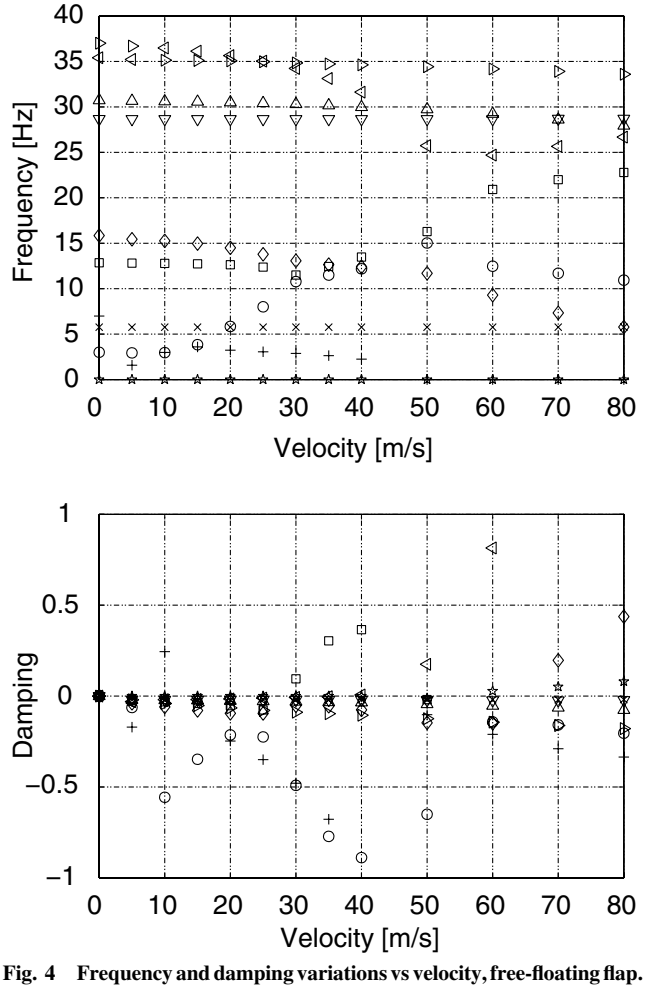


**Fig. 4 Frequency and damping variations vs velocity, free-floating flap.**

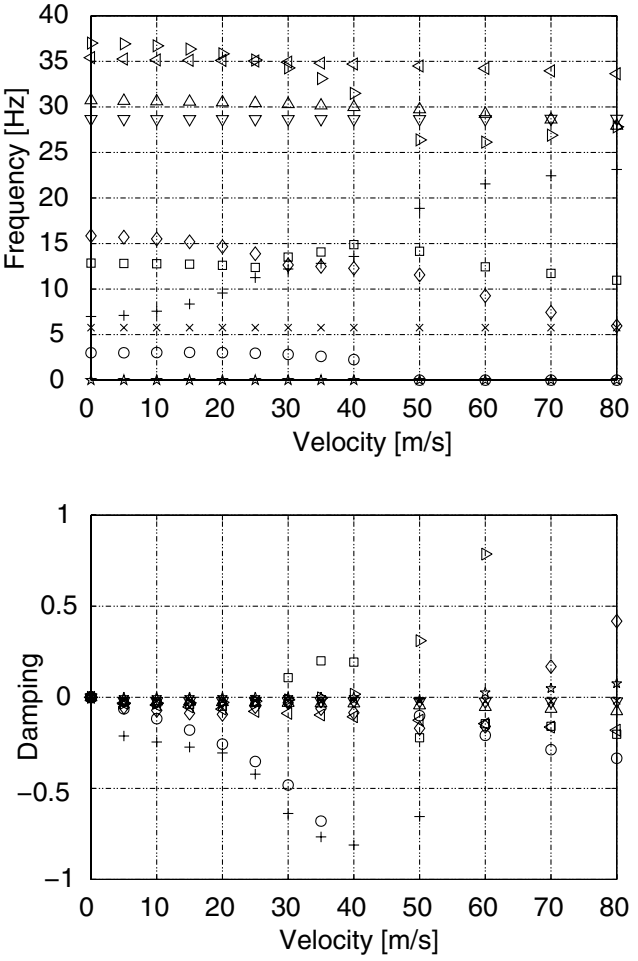


**Fig. 5 Frequency and damping variations vs velocity, flap with rotational stiffness.**

The frequency bandwidth of the PZT response to voltage command is typically much larger that the aeroelastic frequency range of interest [1]. This would allow the modeling of the PZT actuator as a zero-order control law with no delay. However, the control-mode ASE modeling methodology [5] requires the actuator to be modeled as a third-order transfer function for proper inclusion of the control-surface inertial and aerodynamic effects. Hence three states were used for modeling the actuator by

$$T_{\text{ac}}(s) = \frac{a}{a + bs + cs^2 + s^3}$$

with $a = 6.6155 \times 10^9$, $b = 5.2861 \times 10^6$, and $c = 2.8159 \times 10^3$, such that it has a frequency band of more than 300 Hz, which implies a very fast response with practically no delays. The resulting 25-state ASE model was exported for control design using Matlab with the wing-tip acceleration, wing-tip displacement, and aileron rotation angle serving as output parameters, and with the actuator input command serving as an input parameter.

The ASE model was first used for open-loop flutter analysis using the $g$-method [16] of ZAERO. The purpose of the flutter analysis was to investigate the effects of the added flap stiffness (discussed previously) on the open-loop stability characteristics. The variations of the aeroelastic frequency and the nondimensional damping vs air velocity are shown in Fig. 4 for the free-floating flap and in Fig. 5 for the stiffened flap with rotational stiffness. As commonly done in presenting flutter results, all the presented damping values are negative when the system is stable. Flutter occurs when a damping branch becomes positive. The flap rotational frequency increase rapidly with velocity and crosses other modal frequencies. It is marked in the free-floating case of Fig. 4 by pluses (+) up to 5 m/s, then by circles (○) up to 25 m/s, and then by squares. Because the

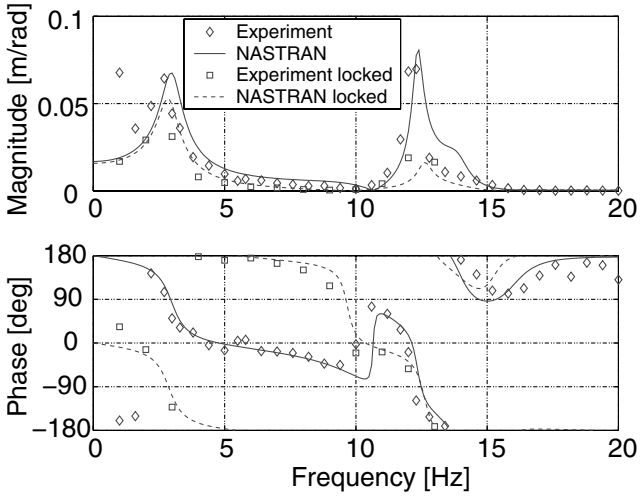


**Fig. 6 Normal displacement at location of accelerometer no. 6.**

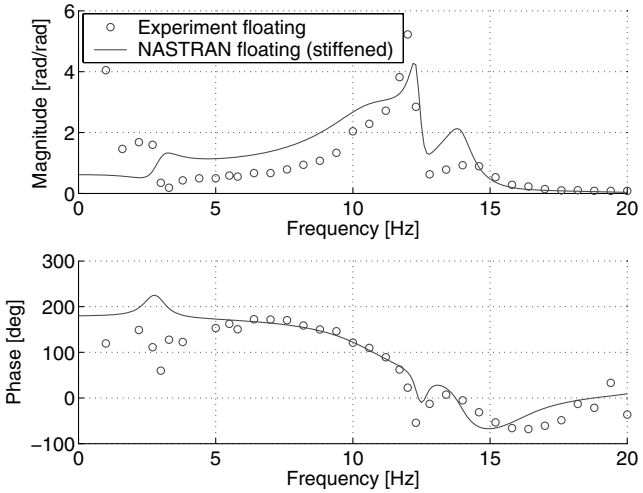


**Fig. 7 Flap deflection.**

flap is underbalanced, it creates two hump flutter mechanisms when its frequency crosses that of the first and second bending modes. It starts in this case with $f = 0$ Hz at $V = 0$ m/s and crosses the first bending frequency at about $f = 3$ and the second bending frequency at about $f = 12$ Hz. As a result, the first bending mode becomes unstable between $V = 7$ and 14 m/s (represented by the positive plus at 10 m/s), and the second bending mode becomes unstable between $V = 28$ and 53 m/s (marked by squares in this range). The rotationally stiffened flap rotational frequency (marked by pluses throughout Fig. 5) starts with $f = 7$ Hz at $V = 0$. It interacts only with the second bending mode (marked by squares) to yield a more moderate hump flutter at 12 Hz between $V = 26$ and 48 m/s. Hence, the stiffened case, which represents the wind tunnel model, is free from flutter in the test velocity range of up to 25 m/s, but its close flutter velocity caused difficulties in the control design, as discussed later.

## Validation Testing

Using the Nastran model, frequency response functions as those determined experimentally were computed. For comparison, the measured actuator strain and accelerations were transformed to tab deflection and displacements, respectively. Magnitude and phase curves displacements in the wing-tip accelerometer and flap deflections to angular deflections of the piezoelectric tab are shown in Figs. 6 and 7 for both simulation and experiment.

Both magnitude and phase angle can be predicted well. For low frequencies, the predictions do not match the experimental data very well, which is expected because the accelerations depend on the square of the frequency and thus the signal-to-noise ratio for this frequency region is fairly low. It is clear that the numerical model is capable of reproducing experimental results in the considered frequency region.

The concept of using the PZT actuator not directly for deflecting a control surface, but rather to amplify the effect by using the floating flap, was investigated. For very low frequencies, the effect of the tab deflection and the resulting flap deflection counteract each other, and there is practically no magnitude gain due to the free-floating flap. For higher frequencies, however, Figs. 6 and 7 show that the magnitude using the locked flap is significantly lower than in the floating case with realistic stiffness and damping. Also, there is a phase difference of 180 deg between the locked and the floating configuration with rotational stiffness, which can be explained by the fact that in the floating case, the flap is deflecting in the opposite direction of the tab. As the excitation frequency exceeds the eigenfrequency of the flap mode, however, the flap starts to deflect in phase with the tab, leading to a vanishing phase difference between the two cases.

A numerical investigation of the floating flap properties was performed. As expected, the magnitude can be significantly increased when decreasing the stiffness of the flap rotational degree of freedom. An investigation of the rotary inertia shows that the bandwidth is reduced as the inertia increases. Therefore, to obtain the largest possible response, a lightweight flap with low stiffness is favorable. This, however, will lead to degradation of flutter properties, because low stiffness and the lack of mass balancing may result in control-surface flutter. In the present case, a reasonable tradeoff was found.

## Active Control for Gust Alleviation

The purpose of this section is to demonstrate the applicability of the smart tab concept for the alleviation of the wing response to discrete (deterministic) gust excitation. It was demonstrated in the previous sections that the actual installation of the piezotab in the wind tunnel, with some stiffness and damping in the flap hinge due to the electric cables, is free from flutter up to $V = 26$ m/s and has a reasonable authority on the flap rotation. However, the early attempts to use this model for gust alleviation at 25 m/s showed that the proximity to the flap flutter speed of 26 m/s caused a severe ASE instability when a controller was added. Hence, it was decided to demonstrate the piezotab capabilities with a free-floating flap that has no rotational stiffness and damping. It is assumed that it is possible to manufacture a floating flap with very low rotational stiffness, and that the flutter of this configuration at 7–14 m/s can be eliminated by some means such as flutter-suppression control laws, mass balancing, or locking the flap in this velocity range.

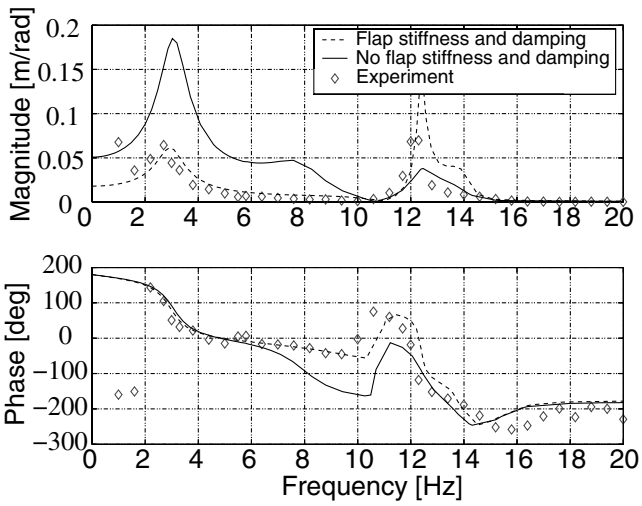


**Fig. 8 FRF of normal wing-tip displacement to tab rotation command, ASE model.**

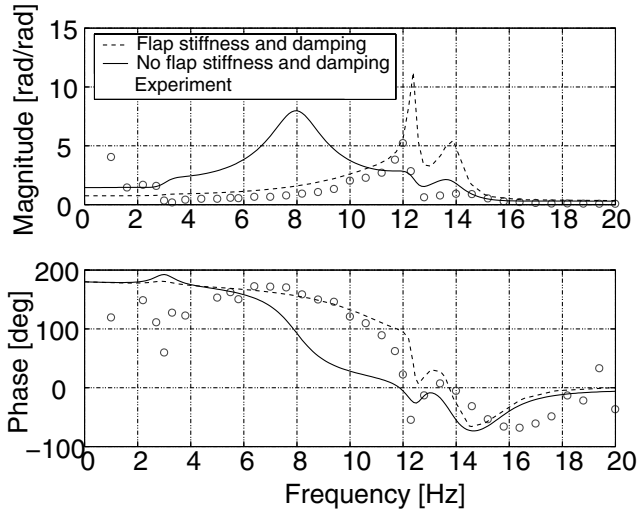


**Fig. 9 FRF of normal flap deflection to tab rotation command, ASE model.**

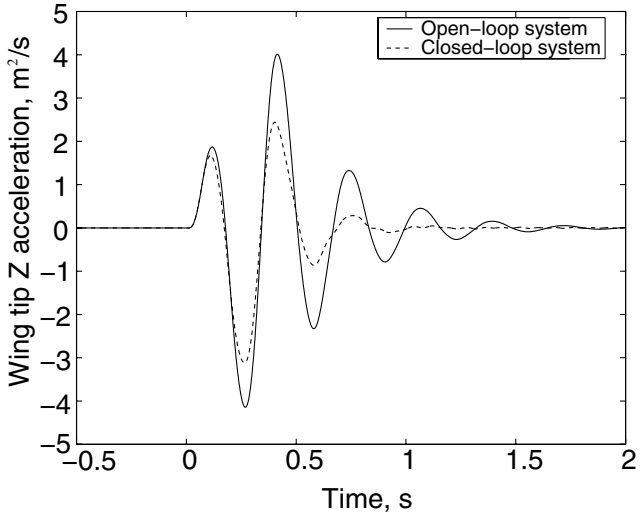


**Fig. 10 Gust-response, wing-tip vertical acceleration.**

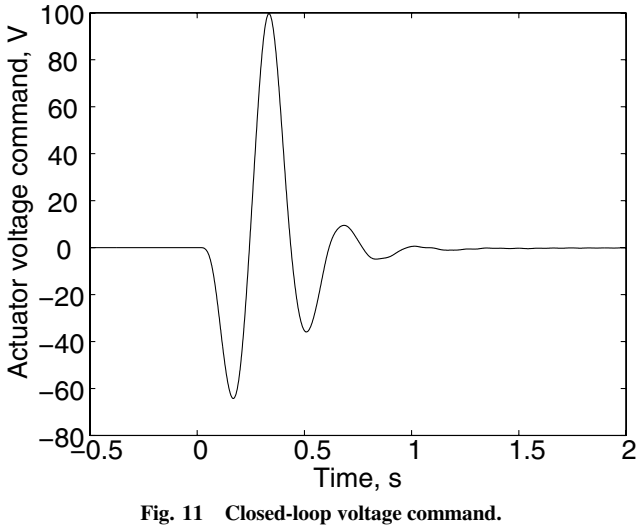


**Fig. 11 Closed-loop voltage command.**

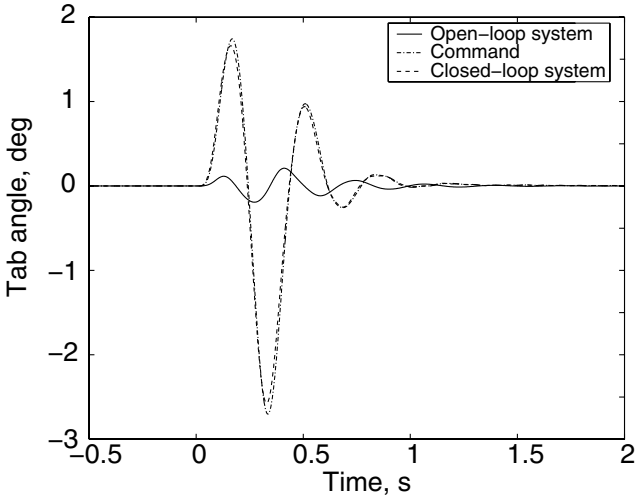


**Fig. 12 Tab deflection.**

The FRFs of the wing-tip displacement and flap rotation to tab excitation, as calculated with the state-space ASE model, are shown in Figs. 8 and 9, respectively. Plots are given in these figures for the flap with and without rotational stiffness and damping. The comparison of the plots with rotational stiffness to the floating cases in Figs. 6 and 7 shows that the differences in the range of 0–11 Hz are insignificant. The responses in the range of 11–15 Hz are also similar, but those obtained with the ASE model are larger than those calculated by Nastran by a factor of 2. The differences are due to differences in the actuator dynamics (stiffness and inertia) and maybe also be due to the slightly different aerodynamic coefficients between Nastran and ZAERO.

Because the system is close to flutter, slight changes in the structural and aerodynamic models can cause large response differences. In any case, since the frequency range of interest for gust-response analysis when the system is stable is up to about 5 Hz, as discussed below, the ZAERO ASE model can be considered as well representing the wind tunnel model. The no-stiffness plots in Figs. 8 and 9 show a significantly larger control authority compared to the ASE cases with stiffness, with much smaller responses at 12–14 Hz due to the larger difference between the flap and the second bending frequencies. The larger control authority and the larger distance from the flutter velocity make the no-stiffness model a better candidate for demonstrating the piezotab gust-alleviation capabilities.

The goal of the control design was to reduce the structural accelerations in response to discrete-gust excitation as much as possible without exceeding the maximal PZT voltage command of

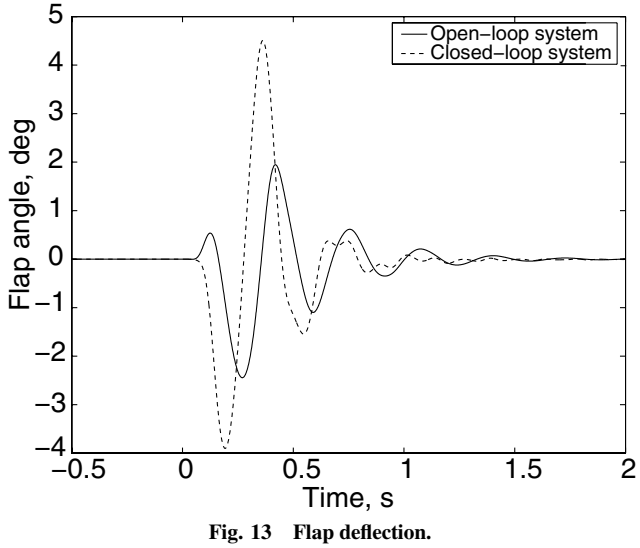


**Fig. 13 Flap deflection.**

100 V and without causing instability at the tunnel velocity of 25 m/s. The main purpose was the demonstration of the piezotab capabilities with the simplest possible control law, which allows physical insight. The test case was the dynamic response to the uniform normal gust velocity profile

$$w_g(t) = \bar{w}_g[1 - \cos(2\pi t/L_g)]/2$$

where $\bar{w}_g = 0.5$ m/s is the maximal gust velocity and $L_g = 0.33$ s is the gust length in terms of the time it passes a point on the wing. The gust length was chosen to be equal to the wavelength of the first bending frequency (3 Hz), which was checked to yield the maximal open-loop acceleration response. The first-order low-pass controller

$$T_c(s) = \frac{k}{Ts + 1}$$

with $k = 280$ and $T = 0.56$ that reads the wing-tip acceleration and commands the PZT actuator was found suitable for demonstrating the tab capabilities.

The time histories of the open- and closed-loop wing-tip acceleration responses and the closed-loop voltage command are shown in Figs. 10 and 11 respectively. It can be observed that the control activity adds a significant damping to the structural response and that the maximal acceleration response (in absolute values) is reduced from 4.1 to 3.1 $m/s^2$, a reduction of 25%, without exceeding the maximal capabilities of the PZT actuator. The fact that the control authority is large at 3 Hz (see Fig. 6) is not just good luck. As for the maximal open-loop response, the authority peak is also associated with the first wing bending frequency.

The time histories of the open- and closed-loop tab and flap deflections are shown in Figs. 12 and 13 respectively. Figure 12 also includes the commanded tab angle, which is the voltage command of Fig. 11 kinematically translated to the tab angle. The small open-loop tab deflection and the small difference between the commanded and actual closed-loop tab deflections are due to the actuator stiffness properties. It can be observed that even though the extreme tab deflection is about 2.6 deg, the flap reaches 4.5 deg, the effect of which on the response accelerations is very significant. This ratio agrees with the corresponding case in Fig. 9 at 3 Hz, the first wing bending frequency.

## Conclusions

The main advantages of piezoelectric actuators are the relatively small size and high bandwidth. For practical applications, however, these actuators are quite restricted due to small actuator stroke and fairly high energy consumption. In the present study, it was shown by both numerical investigations and experiments that the concept of using a piezoelectric actuator along with appropriate aerodynamic amplification is a convenient way of exploiting the actuator. In the present case, the actuator stroke restriction was compensated for by the free-floating flap concept, and yet some bandwith could be preserved. In the present case, the highest performance in terms of frequency response magnitude and bandwidth is obtained by reducing flap stiffness and inertia. Practical issues as well as flutter concerns, however, require some tradeoff. A numerical gust-response investigation demonstrated that simple control laws based on local measurements can be used to alleviate the structural vibrations due to dynamic gust excitations by considerable amounts, 25% in our case. The maximal flap deflection of 4.6 deg obtained with a tab deflection of −2.5 deg is a good demonstration of the aeroelastic leverage that amplifies the effects of the very limited PZT stroke. This research forms the basis for further investigation on the exploitation of the piezotab concept in the alleviation of other gust-response parameters and associated design loads. The demonstrated control authority indicates that such tabs may also be used for flutter suppression and aircraft maneuver enhancements, which requires further research.

## Acknowledgments

All activities were financed by the European Union under the Fifth Framework Programme, through the project *Active Aeroelastic Aircraft Structures*, project number GRD-1-2001-40122. The work was technically supported by Boris Moulin of Technion, and Dan Borglund and John Dunér of the Royal Institute of Technology.

## References

[1] Chopra, I., "Review of State of the Art of Smart Structures and Integrated Systems," *AIAA Journal*, Vol. 40, No. 11, 2002, pp. 2145–2187.

[2] Crawley, E. F., "Intelligent Structures for Aerospace—A Technology Overview and Assessment," *AIAA Journal*, Vol. 32, No. 8, 1994, pp. 1689–1699.

[3] Kurdila, A. J., Li, J., Strganac, T. W., and Webb, G., "Nonlinear Control Methodologies for Hystereis in PZT Actuated On-Blade Elevons," *Journal of Aerospace Engineering*, Vol. 16, No. 4, Oct. 2003, pp. 167–176.

[4] Giurgiutiu, V., "Review of Smart-Materials Actuation Solutions for Aeroelastic and Vibration Control," *Journal of Intelligent Material Systems and Structures*, Vol. 11, No. 7, 2000, pp. 525–544.

[5] Karpel, M., and Moulin, B., "Models for Aeroservoelastic Analysis with Smart Structures," *Journal of Aircraft*, Vol. 41, No. 2, 2004, pp. 314–321.

[6] Heeg, J., "Analytical and Experimental Investigation of Flutter Suppression by Piezoelectric Actuation," NASA TR TP-93-3241, 1993.

[7] Koratkar, N. A., and Chopra, I., "Open-Loop Hover Testing of a Smart Rotor Model," *AIAA Journal*, Vol. 40, No. 8, Aug. 2002, pp. 1495–1502.

[8] William, C., Cooper, J. E., and Wright, J. R., "Force Appropriation for Flutter Testing using Smart Devices," AIAA Paper 2002-1652, 2002.

[9] Schweiger, J., and Suleman, A., "The European Research Project Active Aeroelastic Aircraft Structures," *CEAS/AIAA/NVvL International Forum on Aeroelasticity and Structural Dynamics*, Netherlands Association of Aeronautical Engineers, Amsterdam, 2003.

[10] Eller, D., and Heinze, S., "An Approach to Induced Drag Reduction with Experimental Evaluation," *AIAA Journal of Aircraft*, Vol. 42, No. 6, 2005, pp. 1478–1485.

[11] Midé Technology Corp., Medford, MA, Technical Note for users of the Quickpack Transducer, 2004, www.mide.com.

[12] MSC Software Corporation, Nastran Reference Manual, Santa Ana, CA, 2004.

[13] Albano, E., and Rodden, W. P., "A Doublet-Lattice Method for Calculating Lift Distributions on Oscillating Surfaces in Subsonic Flows," *AIAA Journal*, Vol. 7, No. 2, 1969, pp. 279–285.

[14] Zona Technology, Scottsdale, AZ, ZAERO Theoretical Manual, Ver. 7.2, 2004.

[15] Karpel, M., "Time Domain Aeroservoelastic Modeling Using Weighted Unsteady Aerodynamic Forces," *Journal of Guidance, Control, and Dynamics*, Vol. 13, No. 1, 1990, pp. 30–37.

[16] Chen, P. C., "Damping Perturbation Method for Flutter Solution: the *g*-Method," *AIAA Journal*, Vol. 38, No. 9, 2000, pp. 1519–1524.